Controlling the Thermomechanical Behavior of Nanoparticle/Polymer Films

Dan Zhao,[†] Dirk Schneider,[‡] George Fytas,[‡,§,*] and Sanat K. Kumar[†,*]

[†]Department of Chemical Engineering, Columbia University, 500 West 120th Street, New York, New York 10027, United States, [‡]Max Planck Institute for Polymer Research, Ackermannweg 10, 55128 Mainz, Germany, and [§]Departments of Chemistry and Materials Science & Technology, University of Crete and FORTH, P.O. Box 71110, Heraklion, Greece

ABSTRACT We show that the mesoscale (~200 nm) thermomechanical properties of polymer nanocomposites formed from silica nanoparticles (NPs) and poly(2-vinylpyridine) (P2VP) critically depend on their interfacial structure, which can be controlled by the casting solvent. The composite films are solvent cast from either pyridine (PYR) or methylethylketone (MEK), with uniform NP spatial distribution obtained in both cases. In the films cast from MEK, our previous work has shown that a bound layer of P2VP is formed at the NP surfaces, while no such bound layer is formed when PYR is used as the casting solvent. In PYR as-cast films, Brillouin light scattering reveals a single acoustic phonon with its longitudinal sound velocity increasing with NP loading. This implies a homogeneous mixture of the NP and the polymer on the mesoscopic scales for all compositions examined. However, in the MEK as-cast films, two longitudinal and two transverse acoustic phonons are observed at NP loadings above ~20 wt % (or ~11 vol %), reminiscent of two metastable microscopic phases. The dense microphase is attributed to the bridging of NPs by P2VP chains, whereas for the softer medium, we conjecture that there exists an interfacial lower density P2VP layer whose longitudinal sound velocity barely changes with NP loading. These solvent-induced differences in the (elastic) mechanical behavior disappear upon thermal annealing, suggesting that these nanocomposite interfacial structures in the as-cast state (far from equilibrium) locally approach equilibrium (*i.e.*, near equilibrium after annealing). Consistent with these conclusions, the abrupt decrease of the longitudinal sound velocity with temperature occurs at a single glass transition temperature for the annealed nanocomposites irrespective of the casting solvent used, which assumes only a slightly higher (~5 K at 45 wt % or ~29 vol %) value than that in bulk P2VP. The results emphasize the important role of solvent in determining the interfacial structure of nanocomposites, which can be used to tailor their thermomechanical behavior.

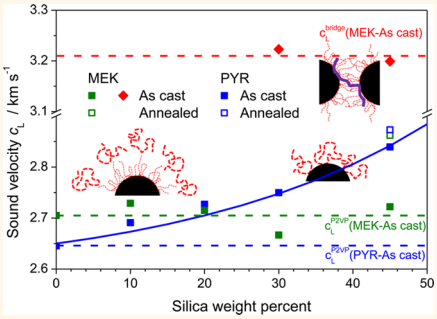

KEYWORDS: Brillouin light scattering · nanoparticle/polymer interface · thermomechanical properties · polymer nanocomposites · solvent effect · glass transition temperature

Polymer nanocomposites (PNCs) have received considerable interest in the past few decades due to the dramatic property improvements that can be achieved upon the addition of a relatively small amount of inorganic nanoparticles (NPs) to a polymer matrix.[1−6] It is now well-accepted that the critical factor leading to these unusual properties is the large surface area inherent in NPs relative to their micron-sized or larger analogues.[7] There are two issues that are controlled by this increased interfacial area (and hence interfacial interactions) in the system: the spatial dispersion of the NPs in the polymer matrix[8−13] and the local interfacial properties,[14−16] such as chain dynamics, and from there the glass transition temperature (T_g) of the nanocomposites. In the community, equilibrium ideas are used to tailor these interfacial interactions, for example, grafting NP surfaces with short ligands (*e.g.*, silane coupling agents)[17] or polymer chains.[18] Bansal *et al.*,[18] for example, used grafted polymer chains to tailor the particle/matrix interface and observed an increase, no change, or decrease in T_g of the resulting PNCs, depending on the wetting behavior of the grafted layer/matrix interface (*i.e.*, wetting, neutral, or nonwetting, respectively).[19]

We suggest that, in addition to these equilibrium ideas, the preparation method by which these composites are created also critically affects the effective interfacial interactions between the NPs and the polymers.[20,21] To be specific, we consider the case of nanocomposites cast from a common solvent. Qualitatively, in a solvent-casting process, the primary factor determining the formation of a bound polymer layer is

* Address correspondence to fytas@mpip-mainz.mpg.de, sk2794@columbia.edu.

Received for review April 29, 2014 and accepted July 29, 2014.

Published online 10.1021/nn503486e

© XXXX American Chemical Society

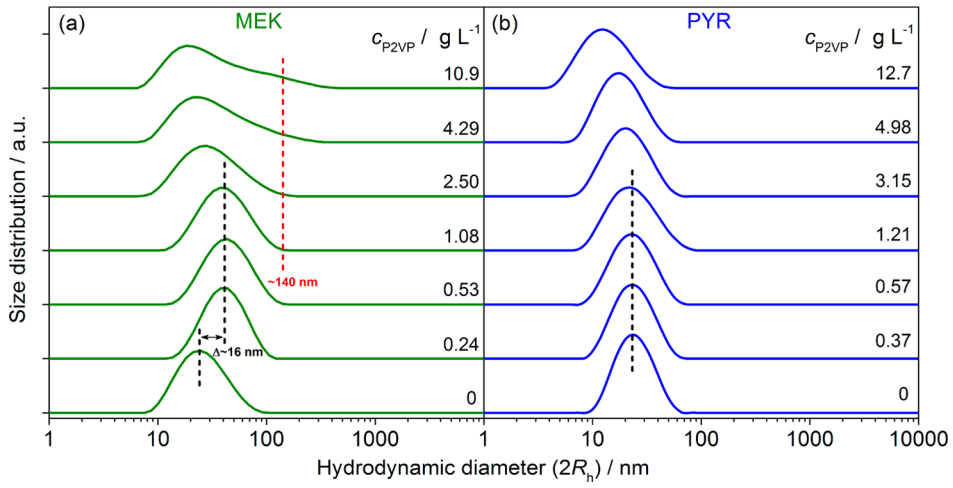

Figure 1. Intensity-averaged hydrodynamic sizes of suspended particles in composite dispersions of (a) MEK and (b) PYR as a function of P2VP concentration, as indicated in the plots. The arrow in (a) denotes a size shift of ~16 nm (~$2R_G$ of 105 kDa P2VP) due to the adsorption of P2VP chains with thickness ~R_G, and the vertical dotted lines are guides for the eye.

the relative interaction strength between the particle/solvent and the particle/polymer, although other factors, such as the bulk thermodynamics of the polymer/solvent mixture, might also be important in some cases. Thus, when the solvent interacts less favorably with the NP surface than the polymer, then the chains strongly absorb onto the particle surface, creating a temporally long-lived bound layer (which can facilitate NP bridging through the bound polymer chains at high particle loadings).[11,14,22−26] At low loadings, the NPs are thus sterically stabilized against agglomeration by the bound layers, leading to uniform NP dispersion. In the opposite case, for which the solvent energetically prefers the NPs, the chains are displaced from the surface, and hence no interfacial bound layer is formed. The NP dispersion then represents a complicated interplay of depletion forces[27,28] (caused by the polymer chains), electrostatic interactions,[29] and van der Waals forces between the NPs.[21,30]

While the relationship between the effective NP−polymer interaction and NP dispersion has been explored to date, in this contribution, we study the relation between the thermomechanical properties and different local structures of the silica/poly(2-vinylpyridine) (SiO_2/P2VP) interface as obtained by different PNC processing conditions, such as solvent casting. We employ Brillouin light scattering (BLS), a noninvasive, noncontact optical technique with spatial resolution in the submicron scale, to measure the elastic moduli (both longitudinal and shear) at different temperatures in both the glassy and rubbery states in the gigahertz frequency range. In the relevant temperature and frequency range, the system behaves as an elastic solid and hence the longitudinal (M) and shear (G) moduli sense local packing and interactions in regions of size comparable to the phonon wavelength ($\Lambda \geq 200$ nm). Going beyond this point, we show that relatively mild thermal annealing (*i.e.*, 7 days at 80 °C followed by 10 days at 150 °C, all under vacuum) can eliminate these solvent effects so that the same, apparently equilibrated, interfacial structures and properties emerge independent of the two solvents used in sample preparation.

RESULTS AND DISCUSSION

The system consists of bare silica NPs with an average core diameter of 14 ± 4 nm and P2VP matrices with a weight-averaged molecular weight of 105 kDa. Films with different NP loadings are solvent cast from either pyridine (PYR) or methylethylketone (MEK), with some samples subjected to a thermal annealing following the procedure described in the Materials and Methods.

NP/Polymer Interaction. Figure 1 presents the hydrodynamic diameter obtained from quasi-elastic light scattering (DLS) from SiO_2/P2VP dispersions in either MEK or PYR as a function of P2VP concentration (C_{P2VP}) at 25 °C. All NP dispersions have the same silica concentration (0.13 wt % or ~0.048 vol %). In the case of pure NPs mixed with solvent (*i.e.*, no polymer), we found that the average hydrodynamic diameter ($2R_h$) obtained from the peaks of inverse Laplace transform (ILT) of the DLS signal is ~23 ± 1 nm in both MEK and PYR, but the width of the size distribution varies due to different sensitivities of the ILT. In MEK, the apparent NP size increases abruptly with the addition of P2VP but then remains virtually insensitive to further increases of C_{P2VP} up to 1.08 g/L (Figure 1a). We conjecture that, in solution, the relative interaction between SiO_2/polymer and SiO_2/solvent determines if a bound polymer layer is formed. Thus, as SiO_2/P2VP interacts much more favorably than SiO_2/MEK, the silica particle adsorbs a monolayer of P2VP chains, with the adsorption being self-limiting due to the lack of additional adsorption sites. The apparent increase in the silica diameter, ~16 nm, matches the diameter (~$2R_G$) of the P2VP ideal coils with $R_G = 6^{-1/2}bN^{1/2}$ ($b = 0.6$ nm

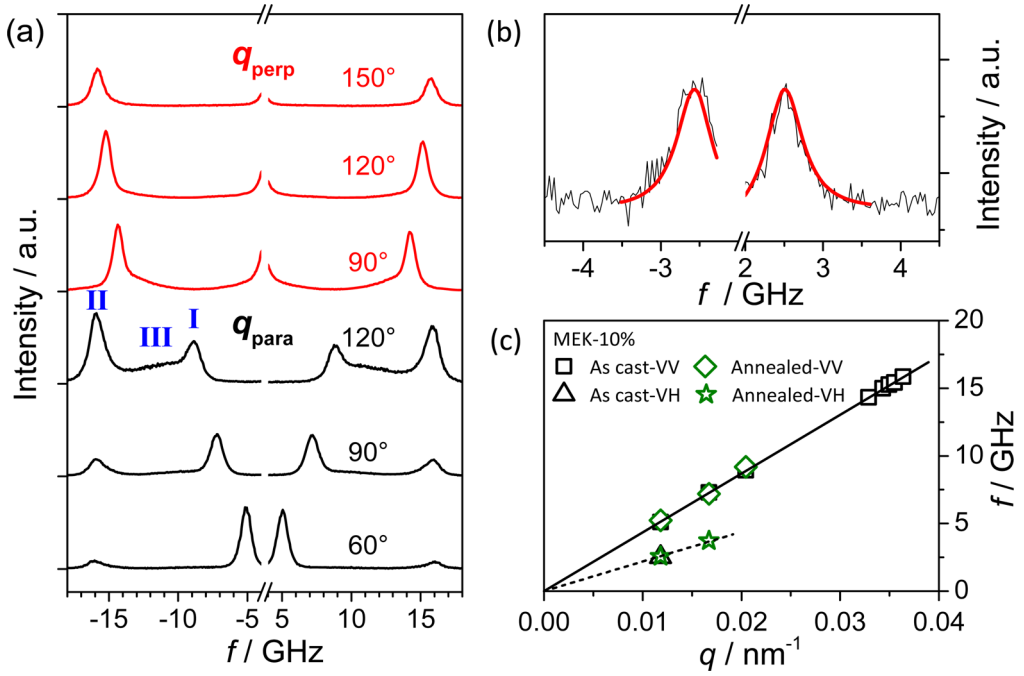

Figure 2. (a) VV-polarized BLS spectra of MEK-10%-as-cast for both in-plane (black) and out-of-plane (red) phonon propagation at a series of scattering vectors as indicated inside the figure. I, II, and III represent the acoustic longitudinal, backscattering, and surface-induced phonons in the transmission geometry. (b) VH-polarized BLS spectra of MEK-10%-as-cast for the in-plane phonon propagation at a scattering vector of $q = 0.0118$ nm^{-1}; in (a) and (b), the central Rayleigh peak region ($\pm$4 GHz for VV spectra and $\pm$2 GHz for VH spectra) have been omitted for visualization purposes. (c) Dispersion relations of MEK-10%-as-cast and MEK-10%-annealed for both longitudinal and transverse acoustic waves, in which the black squares and triangles represent the BLS frequencies of the longitudinal and transverse waves propagating inside the as-cast film and the green diamonds and stars relate to the longitudinal and transverse waves within the annealed sample. The solid and dashed black line is the linear fitting of the phonon frequency *f vs q* for the longitudinal and transverse component of the acoustic phonon, respectively.

and $N = 1000$). The validity of this calculation relies on the fact that MEK is close to a θ-like solvent for P2VP (Figure S1 in Supporting Information).[24] Over a similar P2VP concentration in PYR, the hydrodynamic diameter of silica remains invariant (Figure 1b), implying negligible polymer absorption. Apparently, P2VP chains are displaced away from the silica surface due to stronger SiO_2/PYR interactions.

At C_{P2VP} above ~2.50 g/L in MEK or ~3.15 g/L in PYR, the observed decrease in the hydrodynamic size is apparently due to the progressively larger "free" polymer contribution to the scattering signal. An additional solvent specific behavior is, however, discernible in the size distribution of SiO_2/P2VP in MEK, revealing the presence of larger species with a size larger than 140 nm (dotted red line in Figure 1a) at the two highest polymer concentrations. Since this second population is absent at all P2VP concentrations in PYR and at low P2VP concentrations in MEK, it probably represents silica aggregates, which presumably result from NP bridging through P2VP-bound layers. In fact, when the composite solutions in MEK are left under ambient conditions for long enough time (several weeks), the silica-rich phase with bridging P2VP chains precipitates out from the solution and forms a white layer on the bottom of the glass vial (see Figure S2 in Supporting Information). In contrast, the same silica dispersions in PYR are temporally stable and transparent after several months.

To better understand the different effective interactions between SiO_2/P2VP in MEK and PYR, we refer to our previous work[10] in which we used FTIR, showing that adding a small amount of PYR into a SiO_2/P2VP/MEK system can nearly remove all the MEK from the silica surface. That is, PYR will displace the MEK as it interacts much stronger with the silica surface. Thus, we have strong evidence clearly identifying the different effective interactions between silica and P2VP in the two solvents. Below, we shall investigate these solvent-induced effects in SiO_2/P2VP films solvent cast from either MEK or PYR by probing the propagation of hypersonic thermal phonons using BLS.

Elastic Properties of As-Cast PNC Films. Figure 2 displays representative BLS spectra for a composite film containing 10 wt % silica cast from MEK (MEK-10%-as-cast) at 23 °C at various scattering vectors (q) both parallel (Figure 2b and bottom of Figure 2a) and normal to the film surface (top of Figure 2a). The amplitude of q is tuned by the scattering angle (eq 1 for q_{para} and eq 2 for q_{perp} in Materials and Methods). The VV-polarized spectra in the bottom part of Figure 2a (black lines) consist of the expected acoustic longitudinal phonon (peak I) whose frequency increases linearly with q, as well as a second peak (peak II) with a q-independent

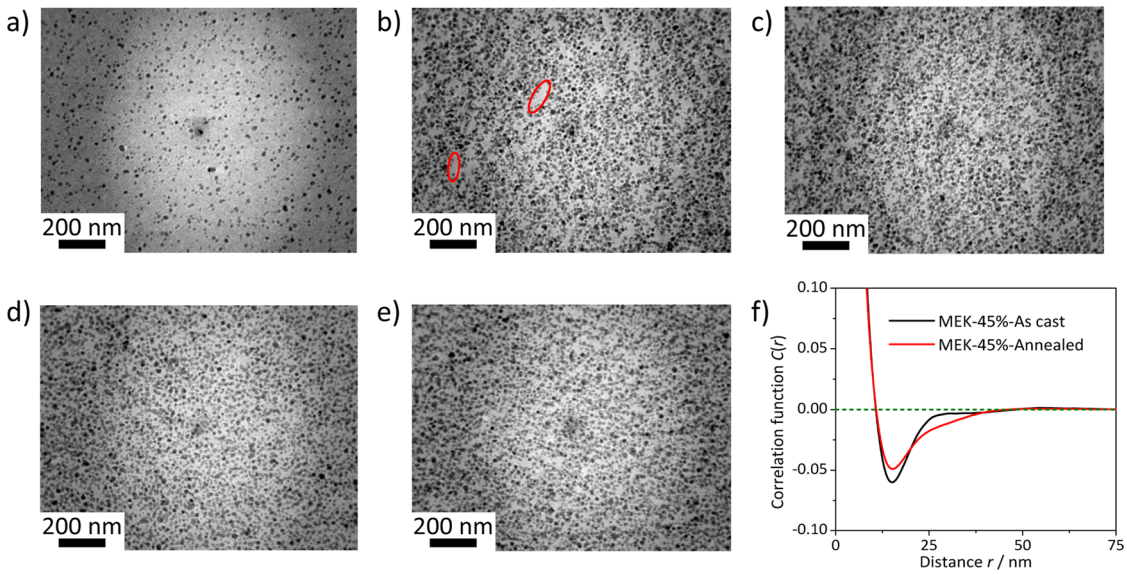

Figure 3. TEM micrographs for (a) MEK-10%-as-cast, (b) PYR-45%-as-cast, (c) PYR-45%-annealed, (d) MEK-45%-as-cast, and (e) MEK-45%-annealed. Also plotted is (f) comparison of autocorrelation function, $C(r)$, of TEM images between as-cast and annealed MEK-45% films, in which each curve is obtained by averaging the correlations of at least 30 TEM images.

frequency; the second peak corresponds to the back-scattering phonon from the laser beam reflected from the exit side of the film. An unexpected broad shoulder (peak III) on the high-frequency side of the acoustic peak can be unambiguously attributed to the surface roughness of the examined films (Figure S3 in Supporting Information). The VV-polarized spectra in the top part of Figure 2a (red lines), collected with q normal to the film surface utilizing the reflection geometry,[31] have a single peak structure. Additionally, the finite optical anisotropy of P2VP allows the measurement of the much weaker VH-polarized spectra (Figure 2b, recorded in the transmission geometry). The single peak spectrum relates to the transverse component of the propagating phonon.

The BLS spectra collectively demonstrate that there is a single acoustic phonon (longitudinal in Figure 2a or transverse in Figure 2b) propagating within this particular sample, indicating spatial homogeneity over the ~200 nm ($\Lambda \sim 2\pi/q$) length scale that is probed. Indeed, TEM images (Figure 3a) show that the silica NPs are individually dispersed in the polymer hosts, with no obvious large particle aggregates or percolating structures visible. In addition, using ImageJ (version 1.45s) on TEM micrograph images, we calculated the average diameter (~12.4 nm) of the particles shown in Figure 3a and also the autocorrelation of the black pixels as a function of distance, $C(r)$ (for details of these calculations, see Figure S4 in Supporting Information). The initial slope of $C(r)$ yields an average particle diameter of ~16 nm. Both quantities confirm the homogeneous nature of particle dispersion within the film.

The linear dispersion relationship for the BLS signal in Figure 2c is valid for thick films ($qh \gg 1$,[32] our thicknesses are $h \sim 100\ \mu$m). Thus, the phonon propagation sound velocities in both the longitudinal (c_L = 2740 ± 30 m/s) and transverse (c_T = 1350 ± 20 m/s) directions are determined from the slopes of corresponding dispersion relations (eq 3 in Materials and Methods), where the peak frequencies are obtained from the representation of the experimental spectra by a Lorentzian function. Access to both c_L and c_T allows estimation of the Poisson ratio, $\nu = (x/2 - 1)/(x - 1) = 0.34$ [with $x = (c_L/c_T)^2$], as well as other mechanical properties, including shear, Young's, and bulk modulus (eqs 4−8 in Materials and Methods). Moreover, since no anisotropy is anticipated for thick films, the linear phonon dispersion should be the same for both in-plane (q_{para}) and out-of-plane (q_{perp}) propagation directions (Figure 2c). This isotropy allows the determination of the refractive index n of the propagation medium, as n affects only the magnitude of q_{perp} (eq 2 in Materials and Methods). Note that the value of ν or n can provide structural and compositional information on the composite medium with the propagating phonon.

As already mentioned, MEK promotes the formation of a P2VP-bound layer in solution, while the particle surface is nearly bald in PYR.[10,24] We now examine the effect of this solvent-induced interfacial modification on the thermomechanical properties of the composite films. Figure 4 shows the longitudinal sound velocities (c_L) in PYR and MEK as-cast samples as a function of silica loading. For reference, we start with the elastic properties of neat P2VP. As indicated by the dashed green and blue lines in Figure 4, there exists a 2.2% difference in c_L of pure P2VP cast from MEK *versus* PYR. This intriguing difference probably arises from the different solvent quality for P2VP in PYR *versus* MEK,

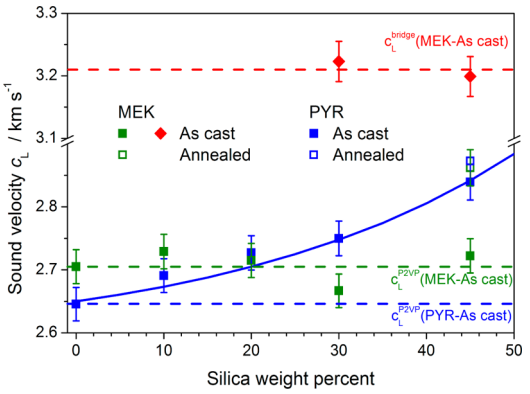

Figure 4. Longitudinal sound velocity (c_L) as a function of silica loading for nanocomposites cast in MEK or PYR. The green (also red) and blue symbols correspond to the nanocomposite films cast in MEK and PYR, respectively. The solid and hollow symbols represent as-cast films and those annealed for 10 days, respectively. The dashed green and blue lines denote the sound velocities of neat P2VP films cast in MEK (c_L = 2710 m/s) and PYR (c_L = 2650 m/s), respectively. The solid blue line is the effective medium prediction for the sound velocities in the PYR-based films. The red diamonds correspond to the fast phonon propagating in the phase of bridged NPs in MEK as-cast films and the red dashed line as a good estimate of the average sound velocity inside this new medium.

which might slightly modify chain packing during the drying process, leading to a small density difference in the as-cast glassy films.

With the addition of silica NPs, in the case of PYR as the casting solvent, there is only one propagating phonon observed for all compositions (see Figure 4 and Figure S6b in Supporting Information). The propagation velocity of this single phonon, c_L (solid blue squares in Figure 4), is reasonably described by Wood's law[33] (solid blue line in Figure 4; see eqs 9 and 10 in Materials and Methods). This indicates that the material follows effective medium theory, implying a uniform film with good "adhesion" between the silica and the P2VP. We conjecture that, even though no P2VP chains adsorb onto the silica surface in the initial solution, P2VP chains gradually approach the particle surface during the drying process as the surface-bound PYR molecules start to be stripped away from the surface. This process apparently leads to a homogeneous mixture of the NPs and the polymer, at least on length scales of ~200 nm. Credence for this statement comes from TEM micrographs (Figure 3b). Clearly, the NPs are almost uniformly distributed in the matrix, with only a small number of particle-sparse regions (indicated by the red circles; the dimension of these white regions is smaller than 200 nm). These small NP-depleted regions (and also presumably aggregates in the same sub-200 nm scale) should be caused by the P2VP-induced depletion forces. However, we believe that the negatively charged nature of the colloidal silica NPs in the initial formulation (with a ζ-potential of −17.8 mV), the short mixing time in solution (~2 h), as well as the increasing viscosity at the later stage of solvent evaporation guarantee a relatively good dispersion throughout the drying process, as observed by Meth *et al.*[29] Unfortunately, due to (i) a relatively poor contrast between silica and P2VP, (ii) the small size of the NPs, and (iii) a two-dimensional projection of multiple layers of particles (the thickness of microtome slices for TEM is ~60 nm), it is difficult to directly visualize the local NP organization in the TEM, especially in the highly loaded samples. In this sense, BLS is a useful indirect tool to help examine the homogeneity of NP dispersion over submicron length scales. To summarize, in PYR as-cast films, the lack of a bound P2VP layer in the solution state, together with the uniform spatial NP distribution, guarantees a single, homogeneous medium for phonon propagation.

In contrast, in MEK as-cast films, c_L (solid green squares in Figure 4) does not depend significantly on the silica loading. Further, at high silica loadings (*e.g.*, 30 and 45 wt %), a second independently propagating phonon is observed—this phonon travels much faster than the first phonon but with a sound velocity nearly independent of the silica loading (top part in Figure 4). Specifically, taking MEK-45%-as-cast as an example, as shown in Figure 5a, we clearly observe two independent phonons for both the in-plane and the out-of-plane spectra, which are normally anticipated only for anisotropic films.[31,34] These phonons are indicated by peaks "I" and "II" inside the plot; peaks "III" and "IV" represent their backscattering counterparts, respectively. This intriguing finding is also supported by the presence of a double-phonon feature in the VH-polarized spectra (see Figure S5 in Supporting Information). Additionally, the recorded dispersion relations for the two different longitudinal and transverse phonons in Figure 5b further confirm the existence of these two different acoustic phonons. Note also that this rules out any anisotropy in the films, which would otherwise scramble the polarization, and the longitudinal phonon scattering will appear in the VH-polarized spectra. Such scrambling is not seen in Figure S5 in Supporting Information. Instead, we conjecture that the presence of two acoustic phonons implies spatial inhomogeneities over a length scale larger than 200 nm for phonon propagation in the MEK as-cast nanocomposites. In such cases, BLS instead acts as a microscopy tool probing regions larger than the phonon wavelength.[34,35] As a result, two longitudinal and two transverse phonons are observed in the VV-polarized and VH-polarized spectra, respectively.

To quantitatively understand the nature of this heterogeneity, we take the sample MEK-45%-as-cast as an example and perform the following three calculations. (i) We find that the Poisson's ratio ν of medium I (corresponding to phonon I in Figure 5) is 0.32, which is close to the value of the pure P2VP (~0.34), while that for medium II (corresponding to phonon II in Figure 5)

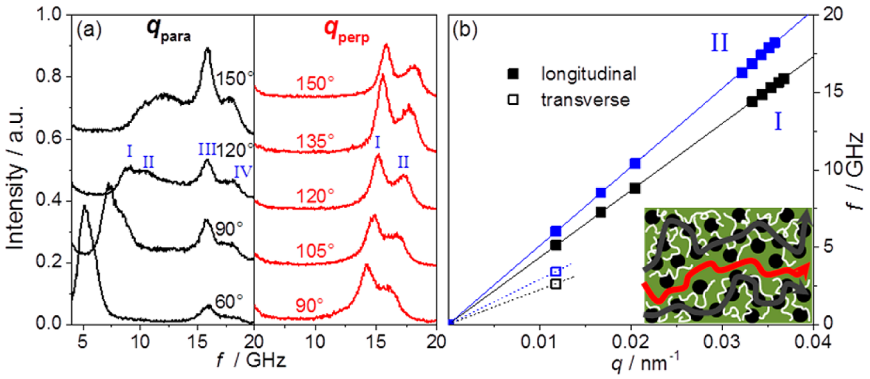

Figure 5. (a) VV-polarized BLS spectra of MEK-45%-as-cast for both in-plane (black, left panel) and out-of-plane (red, right panel) phonon propagation at a series of scattering vectors as denoted by the scattering angles inside the figure. For both in-plane and out-of-plane components, the spectra recorded by shining the incident laser beam from both sides of the film are identical. (b) Dispersion relations of MEK-45%-as-cast for both phonons I and II. The black and blue symbols represent the BLS frequencies of the phonons I and II in (a), respectively. The solid and hollow symbols denote the longitudinal and transverse component of the phonon. The solid and dashed lines denote the linear fits of the frequency of the phonons *f vs q* for the longitudinal and transverse component of the acoustic phonon, respectively. The illustration in the inset of (b) describes the proposed mechanism of an inhomogeneous microseparated structure enabling two phonon propagation with the same *q* in the film of MEK-45%-as-cast, in which only bridging chains (white thin lines) are shown, the black spheres are silica NPs, the black thick lines represent the fast phonon (II) propagation, and the red thick line is the propagating pathway for the slow phonon (I).

is $\nu = 0.26$; note that for normal glass $\nu \sim 0.22$. This implies that medium II is predominantly silica, while medium I is pure P2VP. (ii) The refractive indices *n* related to media I and II are calculated (eq 2 in Materials and Methods) to be 1.578 and 1.535, respectively. This suggests that medium I should be rich in P2VP as its refractive index is within experimental error of neat MEK as-cast P2VP. With *n* for silica being approximately 1.46, the lower *n* for medium II implies that it contains a higher fraction of silica. In fact, assuming the *n* of the composite to be the volumetric average of the components yields a silica loading in medium II of ~54 wt %. (iii) According to the dispersion relation in Figure 5b, the c_L of phonons I and II is estimated to be 2720 and 3200 m/s, respectively. Again, the sound velocity of the phonon I is very close to that of neat MEK as-cast P2VP (c_L = 2710 m/s, as shown in Figure 4). The larger c_L of phonon II indicates a more dense material, that is, more silica. In fact, if effective medium behavior can be assumed, the effective loading of silica in medium II is predicted to be ~55 wt %. These calculations, in total, consistently suggest a two-phase heterogeneous nature in MEK as-cast high loading films, even though the NP dispersion appears to be nominally uniform (Figure 3d).

Next, we address the organization of the NPs within medium II of these heterogeneous composite films. From the DLS solution experiment (Figure 1), we anticipate that NPs in MEK solution are favorably bridged by P2VP chains at high silica loadings. Thus, we assume that the silica-rich medium II in the dry film is inherited from these bridging structures in the solution. Substantiation for this bridging picture comes from the observation that phonon II is only observed for silica loadings larger than 20 wt % (or ~11 vol %) (Figure S6a in Supporting Information). At about this loading, the interparticle separation becomes less than twice the bound layer thickness, that is, $2R_G \sim 16$ nm (see Table S1 in Supporting Information).

Our results suggest the following picture. At low particle loadings, NPs are isolated from each other (Figure 3a), phonon propagation bypasses the NPs and is restricted to the more compressible polymeric phase with a sound velocity approximately equal to that of the neat P2VP (Figure 4) with negligible influence of the harder silica NP component. This also applies to the transverse sound velocity, which thus leads virtually to the same Poisson's ratio as bulk P2VP (*e.g.*, $\nu \sim 0.34$ for the 10 wt % film). Since the sound velocity also depends on the adhesion between the individual components,[36] that is, the force in the harmonic oscillator picture, a virtually composition-independent c_L of phonon I supports the assumption of poor interfacial adhesion between NPs with irreversibly adsorbed polymer chains and the free chains in the bulk. A possible physical picture might be that, at the later stage of solvent evaporation, MEK prefers to go to the bound layer as this will maximize the mixing entropy. At higher loadings, the particle microphase starts to percolate, resulting in a second faster acoustic phonon, which propagates only in the NPs which are locally bridged by the surface-bound P2VP chains. We therefore conclude that the morphology experienced by the acoustic waves corresponds to a "microphase-separated" state, as illustrated in Figure 5b. In the dense NP bridged microdomains, phonons propagate faster (black thick lines) compared to the phonons in the less dense polymer-rich microdomains (red thick line). Thus, the propagation of short wavelength (hypersonic) phonons in nanocomposites can

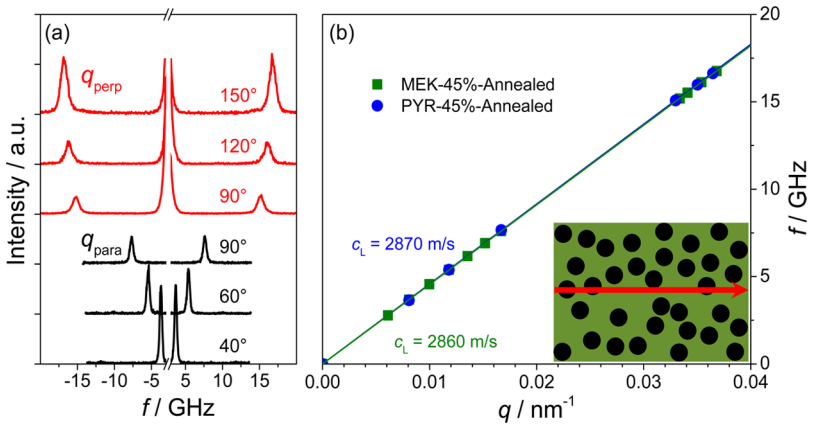

Figure 6. (a) VV-polarized BLS spectra of MEK-45%-annealed for both in-plane (black, bottom) and out-of-plane (red, top) phonon propagation at different scattering vectors as denoted inside the figure. The backscattering modes from in-plane phonon propagation have been omitted for visualization purposes. (b) Dispersion relation *f vs q* for MEK-45%-annealed (green squares) and PYR-45%-annealed (blue circles). The phase velocities in the annealed samples are indicated inside the figure. The inset cartoon in (b) illustrates the effective medium phonon propagation in the annealed film.

sensitively discern microregions with large elastic impedance ($Z = \rho c_L$).[37]

Elastic Properties of Thermally Annealed PNC Films. We now consider the role of thermal annealing on the phonon propagation with particular focus on the two representative loadings cast in MEK: "low" (10 wt %) and "high" (45 wt %). Figure 2c compares the phase velocities of MEK-10%-as-cast and MEK-10%-annealed. Both longitudinal and transverse sound velocities in this film barely change upon thermal annealing, suggesting that the residual solvent (if there is any) in the as-cast film does not affect its intrinsic thermomechanical behavior. In contrast, the thermal history matters for the high-loading nanocomposites as demonstrated for the MEK-45% sample in Figure 6a. Here we observe only one Brillouin peak in each of the in-plane (black lines) and out-of-plane (red lines) VV-polarized spectra. In contrast, two distinct acoustic phonons are resolved in the BLS spectra of the corresponding as-cast film (Figure 5a). This cannot simply be attributed to the complete removal of MEK solvent in the annealing process because, in the case of MEK-10% sample, annealing has no impact on the elastic properties. Instead, we conjecture that the relaxation of the bridging P2VP chains during annealing is at the origin of the different phonon propagation in high loading as-cast and annealed PNCs. A direct implication is the improved mixing of the adsorbed and free chains in the particle–polymer interfacial region on annealing, leading to a much more homogeneous medium as probed by the hypersonic waves. In other words, the local cooperative chain and NP structural rearrangements during annealing diminish the elastic impedance contrast between the two phases in the as-cast films, leading to an effective medium single phonon observation. The fading out of the inhomogeneities is illustrated in the inset of Figure 6b and is supported by the analysis of TEM micrographs in Figure 3, as discussed below.

In Figure 3d,e, TEM micrographs show that the silica NPs are almost uniformly dispersed in the matrices of both as-cast and annealed samples with no obvious particle agglomeration. Although it is difficult to directly characterize the local organization of NPs in the TEM, due to limitations mentioned earlier, the $C(r)$ of the TEM images is still instructive. As presented in Figure 3f, the autocorrelation curves overlap at short distances, indicating that the primary particle diameter (~16 nm) is the same, which further confirms the good dispersion of NPs. The depletion region, characterized by the negative correlation, becomes shallower and wider after annealing, suggesting that the strength of NP–NP repulsion becomes softer but extends to a larger range. We interpret this subtle effect as an indication of the expansion of the adsorbed layer due to the release of the bridging chains between neighboring particles. Thus, the local interfacial structures are able to approach their equilibrium states upon thermal annealing. This is also justified by the nearly identical sound velocity between MEK-45%-annealed and PYR-45%-annealed in Figure 6b; note that the silica NPs are still uniformly dispersed in the P2VP hosts after annealing, as shown in Figure 3c.

In summary, we have shown that the local interfacial structures in both MEK and PYR-cast films can be relaxed with relatively benign thermal annealing within a reasonable experimental time scale. This, together with similar particle morphologies in films cast from these two different solvents, leads to thermomechanical properties that are independent of processing history. We will next provide more evidence for this statement by temperature-dependent experiments.

Glass Transitions in Thermally Annealed PNC Films. As noted above, the annealed SiO_2/P2VP nanocomposites display nearly identical elastic mechanical properties irrespective of the casting solvent used. In glassy polymers, the value of the high-frequency elastic modulus

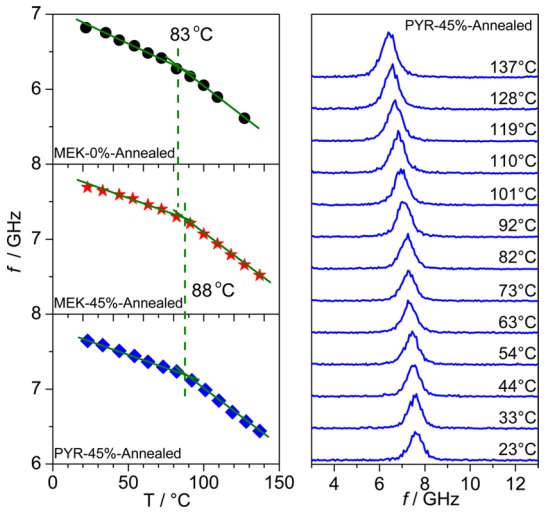

Figure 7. (Left) Brillouin frequencies as a function of temperature within nanocomposite films of MEK-0%-annealed (black spheres), MEK-45%-annealed (red stars), and PYR-45%-annealed (blue diamonds) obtained from temperature scan measurements. The solid green lines represent the linear fitting of *f vs T* in either the glassy or rubbery state. The dashed green lines indicate the small shift in T_g. (Right) Representative Brillouin spectra of PYR-45%-annealed recorded in a typical *T* scan measurement.

depends on the local segmental packing, which changes at the dilatometric glass transition temperature, T_g. We therefore anticipate that T_g should also be independent of the choice of solvent. On the other hand, previous DSC results[10,14] surprisingly showed that nanocomposites consisting of SiO_2/P2VP (with highly attractive interactions) exhibit only a small increase (less than 10 K) in T_g even for particle loadings larger than 60 wt %. We note that DSC probes the relaxation in the specific heat at relatively low rates. Thus, measuring T_g using a different probe, such as BLS, which is sensitive to local packing and interactions, and working at much higher frequencies will provide additional support of the moderate increase of T_g in this PNC. Figure 7 (left panel) shows the temperature dependence of Brillouin peak frequencies (extracted from the BLS spectra isothermally collected at various temperatures, *e.g.*, PYR-45%-annealed, as shown in the right column of Figure 7) in both the glassy and rubbery states. The T_g is defined as the temperature at the intersection of the linear dependences of the longitudinal phonon frequency $f(T)$ in the glassy and rubbery states. The observation of a small T_g increase (~5 K) for both MEK-45%-annealed and PYR-45%-annealed compared to the neat P2VP (Figure 7) is in agreement with the previous DSC results,[14] implying similar interfacial dynamics after removal of solvent-induced effects. A small positive deviation in T_g of PNCs from that of neat polymer was also reported in many other works.[13,29,38,39] Additionally, the annealed bulk P2VP polymer's T_g by BLS (~83 °C) is low compared to its calorimetric value (*i.e.*, ~95 °C).[40,41] Similarly low BLS estimates have also been observed for PS and PMMA.[32] These results are consistent with the results of Efremov *et al.*,[41] who showed that the T_g measured by a nanocalorimetry (characterized by very high heating and cooling rates) for an annealed P2VP thin film is ~84−90 °C).

CONCLUSIONS

In summary, BLS is successfully used to investigate the influence of processing conditions, particularly the choice of the casting solvent and thermal annealing, on the thermomechanical properties of bulk NP/polymer films. When using PYR as the casting solvent, the P2VP chains are displaced away from the particle surface in solution due to the strong interaction between the solvent and the particle. As PYR is evaporated, a homogeneous NP/polymer mixture is created, at least at mesoscopic scales (~200 nm). In these situations, there is a single phonon propagating in all the PYR-cast films, with its sound velocity increasing with the increase of the particle content. These trends are well described by effective medium theory. In contrast, in MEK, a bound P2VP layer has been found at the silica surface in solution, which also facilitates bridging of NPs at higher particle loadings. Due to the poor mechanical adhesion between the particles with adsorbed polymer chains and bulk polymer in the as-cast state, we have found the existence of two propagating phonons, especially at high silica loadings when the particle phase starts to percolate. One phonon propagates in P2VP, while the second independently propagating acoustic phonon is in the region rich in silica NPs locally bridged by P2VP chains. However, upon thermal annealing, the local interfacial structures that are specific to the different solvents used tend to relax within our experimental time scale, leading to an intrinsic elastic modulus and similar interfacial dynamics (characterized by the same T_g) irrespective of the solvent used. Finally, compared to the neat P2VP, the T_g probed by BLS is only slightly increased for nanocomposites with a loading of 45 wt %, which agrees well with our previous DSC results.

MATERIALS AND METHODS

Materials. All materials were used as received. Methylethylketone (HPLC-grade, >99.7%) and pyridine (ACS agent, >99.0%) were purchased from Sigma-Aldrich. P2VP (M_w = 105 kDa, M_w/M_n = 1.08) was obtained from Polymer Source. The colloidal silica NPs (MEK-ST, diameter of 10−15 nm) and the antioxidant Irganox 1010 used in this work were donated by Nissan Chemical Industries and Ciba Specialty Chemicals (now BASF Switzerland), respectively.

Nanocomposite Preparation and Processing. Nanocomposite films were prepared by cocasting composite dispersions consisting

of colloidal silica NPs and P2VP dissolved in either MEK or PYR. First, the as-received Nissan silica suspensions were diluted with the solvent in a volume ratio of 3:7. In the meantime, as-received P2VP and antioxidant Irganox (0.2 wt % relative to P2VP) solutions in MEK or PYR were prepared. Second, appropriate amounts of dilute silica dispersion were added to the polymer/Irganox solution, resulting in silica NP/P2VP formulations with a known weight ratio. The resulting solutions were vortex-shaken for 2 h and then probe-ultrasonicated for 3 min using an ultrasonic processor (model GEX-750) operated at 24% of maximum amplitude with a pulse mode of 2 s sonication followed by 1 s rest. The solutions were then poured into a PTFE Petri dish, air-dried in a fume hood for 2 weeks, and stored in a vacuum oven at room temperature prior to measurements. Each resulting as-cast sample was split into two parts, with one directly sent for BLS measurements and the other subjected to thermal annealing. To provide precisely identical sample history and complete removal of all residual solvents in the films, a well-defined annealing procedure was adopted here: 7 days at 80 °C and then 10 days at 150 °C, both under vacuum. In our notation, sample ID of "PYR (MEK)-10%-annealed (as-cast)" dictates that the film was cast from PYR (MEK) with a silica loading of 10 wt %, which had been (had not been) annealed.

Brillouin Light Scattering. BLS was used to probe the elastic properties of both the as-cast and annealed nanocomposite films. This technique, operating in the gigahertz frequency range, is sensitive to local NP packing and NP/polymer interactions and is capable of addressing directional elastic moduli and dielectric constants,[34] due to the wave vector nature of phonon propagation. The spot size of the incident laser beam is ~50 μm in diameter. As described in our previous studies,[31] the present BLS setup can operate in two different modes, that is, transmission and reflection. In the transmission geometry, the scattering vector q is parallel to the film with its magnitude given by

$$q_{\text{para}} = \left(\frac{4\pi}{\lambda}\right)\sin(\theta/2) \tag{1}$$

where $\lambda = 532$ nm is the wavelength of the incident laser beam in vacuum and θ is the scattering angle. In the reflection mode, the scattering vector q is normal to the film surface and depends on the medium refractive index n *via* a more complex expression, such as eq 12 in ref 42. In this paper, we denote it as eq 2.

$$q_{\text{perp}} = \sqrt{q_{\text{para}}^2 + q_{\text{perp}}^2}\cos\left[\frac{1}{2}\left(\sin^{-1}\left(\frac{1}{n}\sin\alpha\right) - \sin^{-1}\left(\frac{1}{n}\sin(\alpha+\theta)\right)\right)\right] \tag{2}$$

where α is the incident angle.

These two particular configurations allow BLS to selectively characterize either the in-plane or out-of-plane phonons propagating within the test materials. Furthermore, by tuning the polarization of the scattering light, the transverse (also called VH-polarized or depolarized) and longitudinal (VV-polarized or polarized) component of the elastic wave can be decomposed and selectively probed. In a typical BLS measurement, the polarized/depolarized spectrum $I(q,w)$ is recorded as a function of the angular frequency. Following that, the Brillouin frequency, corresponding to the characteristic frequency of the motion of acoustic waves inside the materials, can be extracted by curve fitting the BLS spectra with a Lorentzian function. For acoustic phonons (just as in our case), a linear dispersion relation is obtained

$$c_i = (2\pi f_i)/q \tag{3}$$

where c_i and f_i are the sound velocity and Brillouin frequency of the propagating acoustic phonon, respectively; i can represent either longitudinal (c_L) or transverse (c_T) modes. From here, the propagating sound velocity can be directly calculated. Based on this, other mechanical properties, such as shear, Young's, and bulk modulus, as well as Poisson ratio can be estimated,[43] as given by

$$c_L = \sqrt{\frac{M}{\rho}} \tag{4}$$

$$c_T = \sqrt{\frac{G}{\rho}} \tag{5}$$

$$E = \frac{G(3M - 4G)}{M - G} = 2G(1+\nu) \tag{6}$$

$$K = M - \frac{4}{3}G = \frac{2G(1+\nu)}{3(1-2\nu)} \tag{7}$$

$$\nu = \frac{M - 2G}{2M - 2G} \tag{8}$$

where M, G, E, K, and ν are the P-wave, shear, Young's, bulk modulus, and Poisson ratio, respectively.

Note that all the BLS experiments were performed at room temperature (~23 °C) except for the temperature scan measurements. In the latter, BLS spectra were isothermally collected at representative temperatures ranging from 23 to 137 °C ($\Delta T \sim 10$ K). Prior to each measurement, the whole setup was allowed to isothermally equilibrate for at least 20 min.

The effective medium behavior of the composite film is described by Wood's law, as given by

$$c_{L,\text{PNCs}} = \sqrt{\left(\frac{1}{\phi_{\text{silica}}/(\rho_{\text{silica}}c_{L,\text{silica}}^2) + \phi_{\text{P2VP}}/(\rho_{\text{P2VP}}c_{L,\text{P2VP}}^2)}\right)/\rho_{\text{PNCs}}} \tag{9}$$

$$\rho_{\text{PNCs}} = \phi_{\text{silica}}\rho_{\text{silica}} + \phi_{\text{P2VP}}\rho_{\text{P2VP}} \tag{10}$$

where ϕ_{silica} and ϕ_{P2VP} are the volume fraction of silica and P2VP in the composite film, respectively; $\rho_{\text{silica}} = 1700$ kg/m^3 and $\rho_{\text{P2VP}} = 1100$ kg/m^3 are the densities of the silica NPs and the neat P2VP, respectively; $c_{L,\text{silica}} = 4500$ m/s and $c_{L,\text{P2VP}} = 2650$ m/s are the longitudinal sound velocity of pure silica and P2VP (as-cast in PYR), respectively.

Transmission Electron Microscopy (TEM). To characterize the particle organization in real space, a strip of bulk PNC film was embedded in epoxy resin, cured at 80 °C for 8 h, and then cut into slices with a thickness of around 60 nm using ultramicrotomy which were floated on a Formvar-coated copper TEM grid from deionized water and visualized in a JEOL JEM-100 CX electron microscope.

Dynamic Light Scattering. DLS measurements were performed to obtain the hydrodynamic radii as well as the ζ-potential of suspended particles on a Zetasizer NanoZS (Malvern Instruments) equipped with a 633 nm HeNe laser and operating at a scattering angle of 173° (backscattering setup). In a typical measurement, the stock silica solution (~31 wt %) was first diluted to get a final particle concentration of 0.13% (~0.048 vol %). Following that, appropriate amounts of P2VP were added to this solution based on a given weight ratio. The resulting composite formulation was then stirred on a vortex mixer for at least 1 day to ensure complete polymer dissolution. Finally, the NP size in stable suspension was measured using DLS in a glass cuvette (PCS 1115). Note that the sample was filtered with a 0.45 μm PTFE filter prior to each measurement.

Conflict of Interest: The authors declare no competing financial interest.

Acknowledgment. We thank D. Meng for critical comments and discussions. D.Z. and S.K.K. acknowledge financial support from the National Science Foundation (DMR-1006514). G.F. thanks the European Social Fund and the Greek Ministry of Education (GSRT) in the framework of the program THALIS for financial support.

Supporting Information Available: Scaling of R_h *vs* N for P2VP in MEK; long-term solution phase behavior in MEK or PYR; VV BLS spectra of rough and flat surfaces; autocorrelation function of MEK-10%-as-cast; VH BLS spectra of MEK-45%-as-cast; VV BLS spectra of MEK as-cast films and of PYR-45%-as-cast; interparticle separation as a function of silica loading.

This material is available free of charge *via* the Internet at http://pubs.acs.org.

REFERENCES AND NOTES

1. Winey, K. I.; Kashiwagi, T.; Mu, M. Improving Electrical Conductivity and Thermal Properties of Polymers by the Addition of Carbon Nanotubes as Fillers. *MRS Bull.* **2007**, *32*, 348–353.
2. Kumar, S. K.; Jouault, N.; Benicewicz, B.; Neely, T. Nanocomposites with Polymer Grafted Nanoparticles. *Macromolecules* **2013**, *46*, 3199–3214.
3. Krishnamoorti, R.; Vaia, R. A. Polymer Nanocomposites. *J. Polym. Sci., Part B: Polym. Phys.* **2007**, *45*, 3252–3256.
4. Gilman, J. W. Flammability and Thermal Stability Studies of Polymer Layered-Silicate (Clay) Nanocomposites. *Appl. Clay Sci.* **1999**, *15*, 31–49.
5. Choudalakis, G.; Gotsis, A. D. Permeability of Polymer/Clay Nanocomposites: A Review. *Eur. Polym. J.* **2009**, *45*, 967–984.
6. Cassagnau, P. Melt Rheology of Organoclay and Fumed Silica Nanocomposites. *Polymer* **2008**, *49*, 2183–2196.
7. Schadler, L. S.; Kumar, S. K.; Benicewicz, B. C.; Lewis, S. L.; Harton, S. E. Designed Interfaces in Polymer Nanocomposites: A Fundamental Viewpoint. *MRS Bull.* **2007**, *32*, 335–340.
8. Akcora, P.; Liu, H.; Kumar, S. K.; Moll, J.; Li, Y.; Benicewicz, B. C.; Schadler, L. S.; Acehan, D.; Panagiotopoulos, A. Z.; Pryamitsyn, V.; *et al.* Anisotropic Self-Assembly of Spherical Polymer-Grafted Nanoparticles. *Nat. Mater.* **2009**, *8*, 354–359.
9. Akcora, P.; Kumar, S. K.; García Sakai, V.; Li, Y.; Benicewicz, B. C.; Schadler, L. S. Segmental Dynamics in PMMA-Grafted Nanoparticle Composites. *Macromolecules* **2010**, *43*, 8275–8281.
10. Harton, S. E.; Kumar, S. K.; Yang, H.; Koga, T.; Hicks, K.; Lee, H.; Mijovic, J.; Liu, M.; Vallery, R. S.; Gidley, D. W. Immobilized Polymer Layers on Spherical Nanoparticles. *Macromolecules* **2010**, *43*, 3415–3421.
11. Janes, D. W.; Moll, J. F.; Harton, S. E.; Durning, C. J. Dispersion Morphology of Poly(methyl acrylate)/Silica Nanocomposites. *Macromolecules* **2011**, *44*, 4920–4927.
12. Münstedt, H.; Köppl, T.; Triebel, C. Viscous and Elastic Properties of Poly(methyl methacrylate) Melts Filled with Silica Nanoparticles. *Polymer* **2010**, *51*, 185–191.
13. Jouault, N.; Dalmas, F.; Boué, F.; Jestin, J. Multiscale Characterization of Filler Dispersion and Origins of Mechanical Reinforcement in Model Nanocomposites. *Polymer* **2012**, *53*, 761–775.
14. Moll, J.; Kumar, S. K. Glass Transitions in Highly Attractive Highly Filled Polymer Nanocomposites. *Macromolecules* **2012**, *45*, 1131–1135.
15. Bansal, A.; Yang, H.; Li, C.; Cho, K.; Benicewicz, B. C.; Kumar, S. K.; Schadler, L. S. Quantitative Equivalence between Polymer Nanocomposites and Thin Polymer Films. *Nat. Mater.* **2005**, *4*, 693–698.
16. Sen, S.; Xie, Y.; Kumar, S. K.; Yang, H.; Bansal, A.; Ho, D. L.; Hall, L.; Hooper, J. B.; Schweizer, K. S. Chain Conformations and Bound-Layer Correlations in Polymer Nanocomposites. *Phys. Rev. Lett.* **2007**, *98*, 128302.
17. Becker, C.; Krug, H.; Schmidt, H. Tailoring of Thermomechanical Properties of Thermoplastic Nanocomposites by Surface Modification of Nanoscale Silica Particles. *MRS Online Proc. Libr.* **1996**, *435*, 237–242.
18. Bansal, A.; Yang, H.; Li, C.; Benicewicz, B. C.; Kumar, S. K.; Schadler, L. S. Controlling the Thermomechanical Properties of Polymer Nanocomposites by Tailoring the Polymer–Particle Interface. *J. Polym. Sci., Part B: Polym. Phys.* **2006**, *44*, 2944–2950.
19. Gast, A. P.; Leibler, L. Interactions of Sterically Stabilized Particles Suspended in a Polymer Solution. *Macromolecules* **1986**, *19*, 686–691.
20. Hub, C.; Harton, S. E.; Hunt, M. A.; Fink, R.; Ade, H. Influence of Sample Preparation and Processing on Observed Glass Transition Temperatures of Polymer Nanocomposites. *J. Polym. Sci., Part B: Polym. Phys.* **2007**, *45*, 2270–2276.
21. Sen, S.; Xie, Y.; Bansal, A.; Yang, H.; Cho, K.; Schadler, L. S.; Kumar, S. K. Equivalence between Polymer Nanocomposites and Thin Polymer Films: Effect of Processing Conditions and Molecular Origins of Observed Behavior. *Eur. Phys. J.: Spec. Top.* **2007**, *141*, 161–165.
22. Hooper, J. B.; Schweizer, K. S. Theory of Phase Separation in Polymer Nanocomposites. *Macromolecules* **2006**, *39*, 5133–5142.
23. Kim, S. Y.; Hall, L. M.; Schweizer, K. S.; Zukoski, C. F. Long Wavelength Concentration Fluctuations and Cage Scale Ordering of Nanoparticles in Concentrated Polymer Solutions. *Macromolecules* **2010**, *43*, 10123–10131.
24. Jouault, N.; Moll, J. F.; Meng, D.; Windsor, K.; Ramcharan, S.; Kearney, C.; Kumar, S. K. Bound Polymer Layer in Nanocomposites. *ACS Macro Lett.* **2013**, *2*, 371–374.
25. Surve, M.; Pryamitsyn, V.; Ganesan, V. Polymer-Bridged Gels of Nanoparticles in Solutions of Adsorbing Polymers. *J. Chem. Phys.* **2006**, *125*, 064903.
26. Surve, M.; Pryamitsyn, V.; Ganesan, V. Nanoparticles in Solutions of Adsorbing Polymers: Pair Interactions, Percolation, and Phase Behavior. *Langmuir* **2006**, *22*, 969–981.
27. Asakura, S.; Oosawa, F. Interaction between Particles Suspended in Solutions of Macromolecules. *J. Polym. Sci.* **1958**, *33*, 183–192.
28. Surve, M.; Pryamitsyn, V.; Ganesan, V. Depletion and Pair Interactions of Proteins in Polymer Solutions. *J. Chem. Phys.* **2005**, *122*, 154901.
29. Meth, J. S.; Zane, S. G.; Chi, C.; Londono, J. D.; Wood, B. A.; Cotts, P.; Keating, M.; Guise, W.; Weigand, S. Development of Filler Structure in Colloidal Silica–Polymer Nanocomposites. *Macromolecules* **2011**, *44*, 8301–8313.
30. Jouault, N.; Vallat, P.; Dalmas, F.; Said, S.; Jestin, J.; Boué, F. Well-Dispersed Fractal Aggregates as Filler in Polymer–Silica Nanocomposites: Long-Range Effects in Rheology. *Macromolecules* **2009**, *42*, 2031–2040.
31. Gomopoulos, N.; Saini, G.; Efremov, M.; Nealey, P.; Nelson, K.; Fytas, G. Nondestructive Probing of Mechanical Anisotropy in Polyimide Films on Nanoscale. *Macromolecules* **2010**, *43*, 1551–1555.
32. Cheng, W.; Sainidou, R.; Burgardt, P.; Stefanou, N.; Kiyanova, A.; Efremov, M.; Fytas, G.; Nealey, P. F. Elastic Properties and Glass Transition of Supported Polymer Thin Films. *Macromolecules* **2007**, *40*, 7283–7290.
33. Wood, A. B. *A Textbook of Sound*; Macmillan: New York, 1941.
34. Voudouris, P.; Choi, J.; Gomopoulos, N.; Sainidou, R.; Dong, H.; Matyjaszewski, K.; Bockstaller, M. R.; Fytas, G. Anisotropic Elasticity of Quasi-One-Component Polymer Nanocomposites. *ACS Nano* **2011**, *5*, 5746–5754.
35. Priadilova, O.; Cheng, W.; Tommaseo, G.; Steffen, W.; Gutmann, J.; Fytas, G. Probing the Micromechanical Behavior of Semicrystalline Polypropylene Films by Brillouin Spectroscopy. *Macromolecules* **2005**, *38*, 2321–2326.
36. Liu, Z.; Zhang, X.; Mao, Y.; Zhu, Y.; Yang, Z.; Chan, C.; Sheng, P. Locally Resonant Sonic Materials. *Science* **2000**, *289*, 1734–1736.
37. Sato, A.; Pennec, Y.; Shingne, N.; Thurn-Albrecht, T.; Knoll, W.; Steinhart, M.; Djafari-Rouhani, B.; Fytas, G. Tuning and Switching the Hypersonic Phononic Properties of Elastic Impedance Contrast Nanocomposites. *ACS Nano* **2010**, *4*, 3471–3481.
38. Holt, A. P.; Griffin, P. J.; Bocharova, V.; Agapov, A. L.; Imel, A. E.; Dadmun, M. D.; Sangoro, J. R.; Sokolov, A. P. Dynamics at the Polymer/Nanoparticle Interface in Poly(2-vinylpyridine)/Silica Nanocomposites. *Macromolecules* **2014**, *47*, 1837–1843.
39. Holt, A. P.; Sangoro, J. R.; Wang, Y.; Agapov, A. L.; Sokolov, A. P. Chain and Segmental Dynamics of Poly(2-vinylpyridine) Nanocomposites. *Macromolecules* **2013**, *46*, 4168–4173.
40. van Zanten, J. H.; Wallace, W. E.; Wu, W. Effect of Strongly Favorable Substrate Interactions on the Thermal Properties of Ultrathin Polymer Films. *Phys. Rev. E* **1996**, *53*, R2053–R2056.
41. Efremov, M. Y.; Olson, E. A.; Zhang, M.; Zhang, Z.; Allen, L. H. Probing Glass Transition of Ultrathin Polymer Films at a

Time Scale of Seconds Using Fast Differential Scanning Calorimetry. *Macromolecules* **2004**, *37*, 4607–4616.
42. Schneider, D.; Liaqat, F.; El Boudouti, E. H.; El Hassouani, Y.; Djafari-Rouhani, B.; Tremel, W.; Butt, H.-J.; Fytas, G. Engineering the Hypersonic Phononic Band Gap of Hybrid Bragg Stacks. *Nano Lett.* **2012**, *12*, 3101–3108.
43. Still, T.; Oudich, M.; Auerhammer, G.; Vlassopoulos, D.; Djafari-Rouhani, B.; Fytas, G.; Sheng, P. Soft Silicone Rubber in Phononic Structures: Correct Elastic Moduli. *Phys. Rev. B: Condens. Matter Mater. Phys.* **2013**, *88*, 094102.